

Non-monotonic conductivity of aqueous electrolytes: beyond the first Wien effect

Hélène Berthoumieux,^{1,*} Vincent Démery,^{1,2,†} and Anthony C. Maggs¹

¹UMR CNRS Gulliver 7083, ESPCI Paris, PSL Research University, 75005 Paris, France

²Univ Lyon, ENSL, CNRS, Laboratoire de Physique, F-69342 Lyon, France

(Dated: May 10, 2024)

The conductivity of strong electrolytes increases under high electric fields, a nonlinear response known as the first Wien effect. Here, using molecular dynamics simulations we show that this nonlinear response is non-monotonic for moderately concentrated aqueous electrolytes. We attribute this unanticipated behavior to the fact that, under high electric fields, the permittivity of water decreases and becomes anisotropic. The permittivity tensor measured in the simulations can be reproduced by a model of water molecules as dipoles. We incorporate the resulting anisotropic interactions between the ions into a generalised Stochastic Density Field Theory and calculate ionic correlations as well as corrections to the Nernst-Einstein conductivity which are in good agreement with the numerical simulations.

Almost a century ago, Wien probed the response of strong electrolytes under very high electric fields, up to 0.05 V nm^{-1} . He demonstrated a generic increase of the conductivity upon increasing the electric field, and later found an increase for weak electrolytes; these two phenomena are the first and second Wien effects [1]. Today, fields of up to 0.1 V nm^{-1} are routinely applied in nanofluidic devices involving atomically thin membranes [2, 3], electrodes [4] or channels [5]. Such high fields gave experimental access to the second Wien effect for water dissociation [3] and are also used for the investigation of other ionic transport phenomena including the ionic Coulomb blockade [2], or the creation of ion-based memristors in confined geometries [5, 6].

The first Wien effect was explained by Wilson [7], and later Onsager and Kim, who extended the Debye-Hückel-Onsager (DHO) theory [8, 9] to finite electric fields [10]. According to the DHO theory, ions are surrounded by a cloud of counterions, which is distorted under an external electric field. This distorted cloud generates an additional drag on the ions and reduces their mobility, thereby reducing the conductivity of the solution. Wilson, Onsager and Kim showed that large electric fields destroy the ionic cloud, thus restoring the bare mobility of the ions, which leads to an increase in the conductivity compared to the small field limit.

Recently, the response of strong aqueous electrolytes has been investigated using molecular dynamics (MD) simulations, and a conductivity plateau up to electric fields of 1 V nm^{-1} has been found. Applying the electric field on the ions only, and not on the water molecules, a large increase in the conductivity has been recovered [11, 12]. These results suggest that the molecular properties of water also affect the nonlinear response of electrolytes. However, most of the theoretical efforts from the DHO theory, such as its recent reformulation using Stochastic Density Field Theory (SDFT) and its extensions [13–19] or approaches based on the Mean Spherical

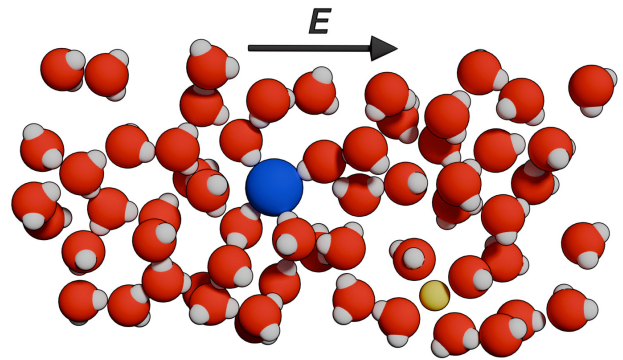


FIG. 1. Snapshot of the classical MD simulations with an electric field of 0.5 V nm^{-1} . The sodium and chloride ions are represented by a yellow and a blue sphere, respectively. The orientation of the water molecules by the external field (black arrow) is clearly visible.

Approximation [20], have focused on a better description of the ions, leaving aside the molecular properties of the solvent. The external field polarizes water by aligning the dipoles of water molecules (Fig. 1) and affects two important water properties for ion transport, making them anisotropic: its permittivity [21–24] and its viscosity [25–28]. Classical MD simulations report that even at high field strengths of 1 V nm^{-1} , the increase in viscosity remains moderate [28], while the permittivity decreases by an order of magnitude [23].

Here we show that the field-induced decrease in water permittivity leads to an increase in ion-ion interactions and compensates for the Debye cloud destructuring. In addition, we find that for a certain range of electrostatic fields and electrolyte concentrations, the cloud enhancement effect induced by the permittivity drop is dominant, resulting in a nonmonotonous conductivity. We use a model of water as dipoles on a lattice [21, 29] to encode the molecular properties of water in a field-dependent, anisotropic, permittivity tensor. We then incorporate this permittivity tensor into SDFT to obtain the ionic correlations and the conductivity of the solution, which

* helene.berthoumieux@espci.psl.eu

† vincent.demery@espci.psl.eu

is nonmonotonic in the electric field. We show that the nonlinear response is controlled by the interplay of two characteristic electric fields: the electric field E_c where the ionic cloud is destroyed for a constant permittivity, and the electric field E_w needed to orient the water molecules. Last, while the main effect is due to the permittivity drop, the permittivity anisotropy significantly affects the conductivity.

We ran classical MD simulations to measure the conductivity of solutions of NaCl in SPC/E water [30–32], at moderate concentrations $\rho = 75$ mM and 150 mM and at temperature $T = 300$ K [33] (App. A). We measured the conductivity for electric fields ranging from 0.025 V nm $^{-1}$ to 0.7 V nm $^{-1}$. At these field amplitudes, some of the water molecules align their dipole moment along the field, but the system retains its liquid structure and the field does not disrupt the ion solvation layers (Fig. 1). The conductivity as a function of E is presented by filled circles in Fig. 2. At both concentrations, the conductivity dependence on the electric field is nonmonotonic: it increases with the electric field up to roughly 0.1 V nm $^{-1}$, and then it decreases slightly with the electric field. While the decay is perceptible in the data of Ref. [12], the initial increase has not been observed. To probe the effect of the alignment of the water molecules on the external field, we performed simulations where the external field has only been applied to the ions [12] (Fig. 2, open squares). In this configuration, the conductivity increases over the whole range of applied electric fields, corresponding to the first Wien effect. For both concentrations, the data are quantitatively reproduced by the DHO theory, without any fitting parameter (Fig. 2, dashed lines).

From the observations above, we conclude that the nonmonotonicity of the conductivity is rooted in the response of the water molecules to the external field. Indeed, the external field polarizes water (Fig. 1), thereby reducing the response of water molecules to extra fields such as the ones generated by the ions, that is, reducing the permittivity of the medium. Computing this effect from first principles has proven a difficult task [34]. Instead, we use a model where the water molecules are represented by dipoles on a lattice with magnitude p and density ρ_d [21, 29], and allow ourselves to fit these quantities [35]. Neglecting the interactions between the dipoles, the free energy density under an external field with magnitude E is

$$f(E) = -\frac{\epsilon_0}{2} E^2 - \frac{\rho_d}{\beta} \log \left(\frac{\sinh(\beta p E)}{\beta p E} \right), \quad (1)$$

where ϵ_0 is the vacuum permittivity and β is the inverse thermal energy. While Ref. [29] focused on one-dimensional systems, the tensorial permittivity may be obtained as $\epsilon_{\mu\nu} = -\partial^2 f(E)/(\partial E_\mu \partial E_\nu)$ [36]. Here, the relevant permittivity to describe the interaction between the ions is given by the expansion of this relation around the external field, leading to a diagonal permittivity tensor with different values along the external field and

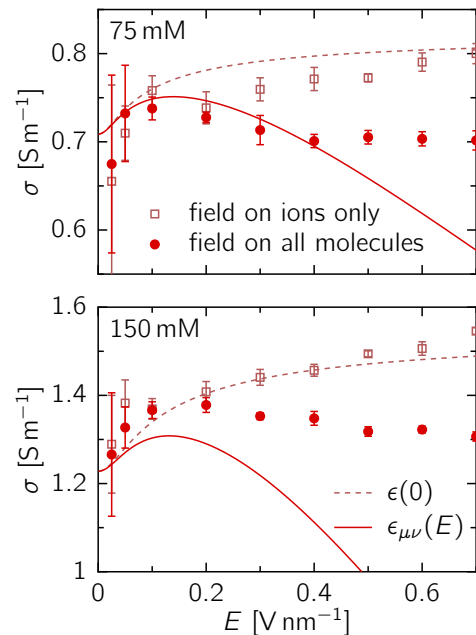


FIG. 2. Conductivity as a function of the electric field for aqueous solutions of NaCl at concentrations $\rho = 75$ mM and 150 mM from numerical simulations (symbols) and theory (lines). Open symbols correspond to simulations where the external electric field is only applied to the ions, while it is applied to the ions and the water molecules for closed symbols. Dashed lines are the DHO theory, with a constant water relative permittivity of $\epsilon_r = 71$; solid lines are the theory described here, which includes the effect of the electric field on the permittivity (Eqs. (4, 5)).

transverse to it:

$$\epsilon_{\parallel} = \epsilon_0 + \rho_d \beta p^2 \left[\frac{1}{x^2} - \frac{1}{\sinh(x)^2} \right], \quad (2)$$

$$\epsilon_{\perp} = \epsilon_0 + \rho_d \beta p^2 \left[\frac{\coth(x)}{x} - \frac{1}{x^2} \right], \quad (3)$$

where $x = \beta p E = E/E_w$ is the dimensionless field, $E_w = 1/(\beta p)$ being the external field necessary to orient a water molecule. Both expressions give $\epsilon_0 + \beta \rho_d p^2 / 3 = \epsilon_0 \epsilon_r$ for small fields and decay to ϵ_0 for large fields.

We simulated a solution of pure water under an increasing electrostatic field from 0 to 1 V nm $^{-1}$ applied along the x direction. We computed the permittivity tensor from the fluctuations of the total dipole moment \mathbf{M} of the simulation cell (App. A 2). The longitudinal permittivity ϵ_{\parallel} is derived from the fluctuations of M_x and the transverse one ϵ_{\perp} from the fluctuations of M_y and M_z . Analytical expressions fit very well to the longitudinal and transverse permittivities measured in the simulations with $p = 3.6 \times 10^{-29}$ C m and $\rho_d = 6.0$ nm $^{-3}$ (Fig. 3), that is, with a dipole moment that is about 5 times larger than that of the water molecule, and a density that is about 5 times smaller than that of the liquid. With this value of the dipolar moment p , the character-

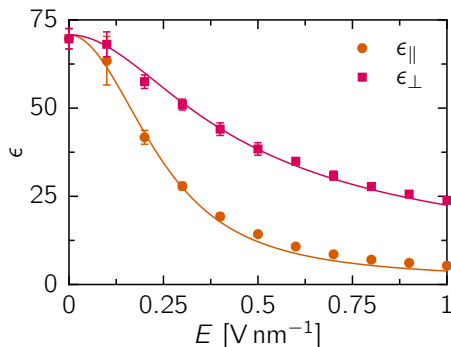


FIG. 3. Longitudinal and transverse permittivity from numerical simulations (symbols) and theory (solid lines, Eqs. (2,3)).

istic field is $E_w \simeq 0.12 \text{ V nm}^{-1}$. Beyond the decay, the permittivity tensor exhibits a strong anisotropy at intermediary fields, the transverse component being much larger than the longitudinal one.

We assume that the permittivity in moderately concentrated electrolytes can be approximated by that of pure water (Fig. (3)). Its anisotropy results in anisotropic electrostatic interactions between the ions: the pairwise interaction between ionic species i and j is given by $\tilde{V}_{ij}(\mathbf{k}) = q^2 z_i z_j / (\epsilon_{\parallel} k_{\parallel}^2 + \epsilon_{\perp} k_{\perp}^2)$ in Fourier space, where q is the elementary charge and z_i is the valency of the ions of type i , \mathbf{k} is the wavenumber and k_{\parallel} and k_{\perp} are its components parallel and perpendicular to the external field, respectively. We resort to SDFT to compute the ionic correlations. The ions are represented as point particles obeying an overdamped Langevin dynamics with mobilities κ_i under the action of the interparticle forces calculated from V_{ij} and the external field \mathbf{E} . Using SDFT, the microscopic dynamics of the ions is mapped onto an overdamped Langevin dynamics for the density field of each species [13]. Assuming small density fluctuations, which corresponds to the Debye-Hückel approximation, the density dynamics can be linearized and the correlations can be computed [14] (App. B).

The Nernst-Einstein conductivity $\sigma_0 = \rho q^2 \kappa$, where $\kappa = \kappa_1 + \kappa_2$, is reduced by the electrostatic $\Delta\sigma_{\text{el}}$ and hydrodynamic $\Delta\sigma_{\text{hyd}}$ corrections, which are deduced from the ionic correlations [14, 17, 37]:

$$\frac{\Delta\sigma_{\text{el}}}{\sigma_0} = -\frac{\beta q^2 m}{4\sqrt{2}\pi\epsilon_0\epsilon_r} \int_0^1 dz \frac{z^2 \gamma_z}{\alpha_z^{3/2}}, \quad (4)$$

$$\frac{\Delta\sigma_{\text{hyd}}}{\sigma_0} = -\frac{m}{2\sqrt{2}\pi\eta\kappa} \int_0^1 dz \frac{(1-z^2)(1+\gamma_z)}{\sqrt{\alpha_z}}. \quad (5)$$

We have introduced the inverse Debye length at zero field $m = \sqrt{2\beta q^2 \rho / (\epsilon_0 \epsilon_r)}$. The anisotropic permittivity is encoded in $\alpha_z = [\epsilon_{\parallel} z^2 + \epsilon_{\perp} (1-z^2)] / (\epsilon_0 \epsilon_r)$ and $\gamma_z = \left[1 + \sqrt{2(1+F^2 z^2 \alpha_z)}\right]^{-1}$. The dimensionless electric field is defined by $F = E/E_c$, where $E_c = m/(\beta q)$ is the field necessary to destroy the ionic cloud when the

permittivity is assumed to be constant. The ionic mobilities κ_i are measured via the Einstein relation in simulations of very dilute solutions without external field (App. A 4). The hydrodynamic correction involves the viscosity η of the solvent, which we assume to be constant and isotropic; we use the value $\eta = 0.729 \times 10^{-3} \text{ Pa s}$ [31]. These expressions hold for monovalent salts; the general results are given in App. C and D.

Our prediction for the conductivity, $\sigma_0 + \Delta\sigma_{\text{el}} + \Delta\sigma_{\text{hyd}}$, is shown by red solid lines in Fig. 2. For comparison, the DHO prediction, which assumes a constant isotropic permittivity $\epsilon_0 \epsilon_r$, is shown as light dashed lines. The agreement is quantitative for the smaller concentration, $\rho = 75 \text{ mM}$; for the larger concentration, $\rho = 150 \text{ mM}$, the theory underestimates the conductivity, as expected [17], but the agreement is still qualitative. The conductivity predicted by DHO is an increasing function of the electric field, as measured in the simulations where the external field acts only on the ions. In contrast, our calculation predicts the nonmonotonic dependence observed in the simulations where the external field acts on all the molecules; in particular, the electric field where the conductivity is maximal is well predicted by the theory. For large electric fields, the discrepancy between theory and simulations increases: as the permittivity decays, the correlations between the ions increase and the assumption of small density fluctuations, used to compute the correlations no longer holds.

To better understand the shape of the conductivity curve, we plot the theoretical prediction for the total correction, $\Delta\sigma = \Delta\sigma_{\text{el}} + \Delta\sigma_{\text{hyd}}$, as solid lines for a wide range of concentrations and a wide range of external fields, up to unrealistic values, in Fig. 4(a). For the most dilute system, $\rho = 15 \text{ mM}$, the correction first decays, which corresponds to an increase of the conductivity, and then increases; for the densest system, $\rho = 1.5 \text{ M}$, the contrary is observed: the correction first increases and then decays. In the intermediate range, for instance for $\rho = 150 \text{ mM}$, the correction decreases, increases and decreases again; the last decay is not observed in Fig. 2 as it occurs for large values of the external field, $E \gtrsim 10 \text{ V nm}^{-1}$. Two nonlinear effects compete here; one is the decay of the water permittivity, which enhances the interactions and the ionic correlations, occurring at the characteristic field E_w . The other is the destruction of the ionic correlations above the characteristic field E_c . For weak electric fields, the evolution of the conductivity is the sum of the two effects (App. C 3 and D 3):

$$\frac{\sigma(E) - \sigma(0)}{\sigma_0} \underset{E \rightarrow 0}{\sim} a \frac{E^2}{E_c^2} + b \frac{E^2}{E_w^2}. \quad (6)$$

The coefficients a and b scale as $\sqrt{\rho}$ and have opposite sign, $a > 0$ while $b < 0$. The characteristic field E_c also scales as $\sqrt{\rho}$, while E_w is a characteristic of pure water and does not depend on the salt concentration. As a consequence, the coefficient of E^2 in Eq. (6) may change sign as a function of the salt concentration. This

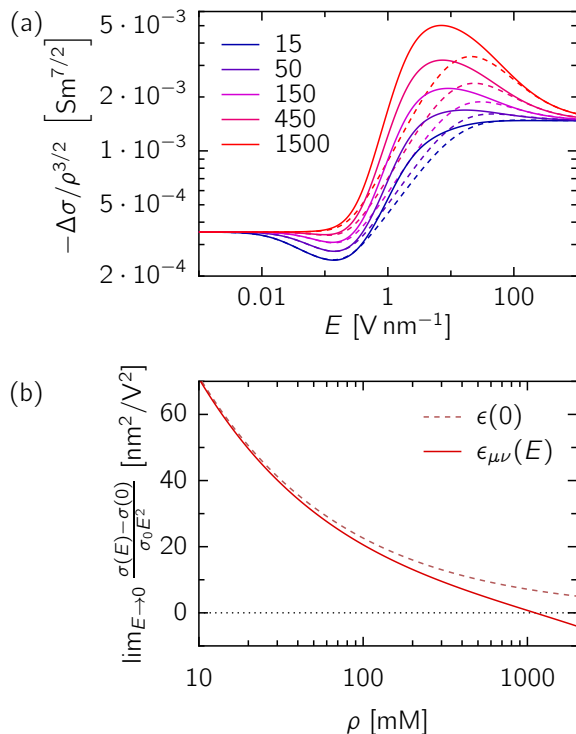


FIG. 4. (a) Rescaled correction to the Nernst-Einstein conductivity for different concentrations (indicated in mM), with the anisotropic permittivity (solid lines) and the isotropic permittivity $\epsilon = \epsilon_{\mu\mu}/3$ (dashed lines). (b) Coefficient of E^2 in the small field expansion as a function of the salt concentration.

is shown in Figure 4(b) where we plot this coefficient as a function of ρ for solutions associated with field-dependent permittivity (solid line) versus solutions with constant permittivity (dashed line). The change of sign occurs for concentrated solutions ($\rho \geq 1$ M), however note that the correction due to the decrease of the permittivity is barely visible for concentrations below 100 mM.

The nonmonotonic evolution of the conductivity with the external field is chiefly explained by the interplay of the destruction of the ionic correlations and the decay of the permittivity, irrespective of its anisotropy. However, considering an isotropic medium by replacing the anisotropic permittivity $\epsilon_{\mu\nu}$ by its angular averaged value $\epsilon_{\mu\mu}/3$ significantly reduces the correction $\Delta\sigma$, which is shown by the dashed lines in Fig. 4.

We have shown that the conductivity of aqueous electrolytes may be a nonmonotonic function of the external field, and we have explained the result by the evolution of the permittivity of water, which decreases with field strength and also becomes anisotropic. The decrease as well as the anisotropy of the permittivity can be included in SDFT to reproduce qualitatively the evolution of the conductivity, and even yield quantitative predictions at low concentrations. In the future, this integration of molecular properties of water into the analyti-

cally tractable framework of SDFT could be extended to include, for instance, a non-local permittivity $\tilde{\epsilon}(\mathbf{k})$ to account for the finite size of the water molecules [38]. Finally, beyond the bulk conductivity of strong electrolytes, we expect that the molecular properties of water also affect ionic transport in quasi two- or one-dimensional systems, where confinement and ions control the structure of water [39]. This results in a strongly anisotropic permittivity tensor, which values can be significantly higher [40] or lower [39, 41] than the bulk one. The inclusion of the molecular properties of the solvent in SDFT would thus allow a better description of the first and second Wien effects in such systems [5, 6].

Appendix A: Molecular dynamic simulations

1. Simulation methods

Simulations are performed using the GROMACS 2021 molecular dynamics simulation package [33]. Simulation boxes are periodically replicated in all directions, and long-range electrostatics are handled using the smooth particle mesh Ewald (SPME) technique with tin-foil boundary conditions. Lennard-Jones interactions are cut off at a distance $r_{\text{cut}} = 0.9$ nm. The potential is shifted to zero at the cut-off separation. All systems are coupled to a heat bath at 300 K using v-rescale thermostat with a time constant of 0.5 ps. We use MDAnalysis to treat the trajectories.

After creating the system, we first perform energy minimization. We then equilibrate the system in the NVT ensemble for 200 ps, and then in the NPT ensemble for another 200 ps using a Berendsen barostat at 1 bar. Production runs are performed in the NVT ensemble for 20 ns or 40 ns in the case of mobility measurement. The integration time step is set to $\Delta t = 2$ fs.

2. Permittivity of pure water under electrostatic field

We simulate a cubic box of pure water of side size $L = 6.5$ nm. We use the SPC/E model for water [30, 31]: a three-point charge, and one Lennard-Jones reference site model. The Lennard-Jones (LJ) center is placed on the oxygen. Charges are placed on the hydrogen atoms and the oxygen.

During the production run, we apply a static electrostatic field along the x -axis to the system using the option “electric-field-x: E 0 0 0”. We perform 11 production runs varying the amplitude of E from 0 to 1 V nm⁻¹ with a step of 0.1 V nm⁻¹.

In an external field, the permittivity of water is an anisotropic, diagonal tensor characterized by a component ϵ_{\parallel} , aligned with the field direction x , and a perpendicular component ϵ_{\perp} in the (y, z) plane. We calculate this tensor from the total system dipole moment [42] \mathbf{M}

that we compute for each frame after dropping the first nanosecond of the run. It is defined as the volume integral of the polarization \mathcal{P} , $\mathbf{M} = \int_V \mathcal{P}(\mathbf{r})d\mathbf{r}$, where V is the volume of the box. The permittivity obeys:

$$\epsilon_{\parallel} = \frac{\langle M_x^2 \rangle - \langle M_x \rangle^2}{\epsilon_0 k_B T V} + 1, \quad (\text{A1})$$

$$\epsilon_{\perp} = \frac{\langle M_y^2 \rangle + \langle M_z^2 \rangle - \langle M_y \rangle^2 - \langle M_z \rangle^2}{2\epsilon_0 k_B T V} + 1. \quad (\text{A2})$$

3. Field-dependent conductivity of aqueous electrolyte solution

We simulate a cubic aqueous electrolyte box of size $L = 6.5$ nm. The 150 mM solution contains 8875 water molecules and 25 ion pairs of (Na^+ , Cl^-), the 150 mM solution contains 8901 water molecules and 12 ion pairs. The Debye length of the electrolyte is equal to 0.7 nm, respectively 1.1 nm, which is significantly smaller than the box size. We take the following LJ parameters ($\sigma_{\text{Na}} = 0.231$ nm, $\epsilon_{\text{Na}} = 0.45$ kJ mol $^{-1}$) and ($\sigma_{\text{Cl}} = 0.43$ nm, $\epsilon_{\text{Cl}} = 0.42$ kJ mol $^{-1}$) [32] and we use the Lorentz-Berthelot mixing rules for the LJ interactions.

For the first set of simulations, we proceed as for pure water and apply a static electrostatic field along the x -axis during the production run. We perform 9 runs for which we vary the amplitude of E from 0.025 V nm $^{-1}$ to 0.7 V nm $^{-1}$.

For the second set of simulations, only the ions (Na^+ , Cl^-) feel the electrostatic field, and not the water charges. We impose an acceleration $a_{\text{Na}} = qE/m_{\text{Na}}$ to the cations and $a_{\text{Cl}} = -qE/m_{\text{Cl}}$ to the anions along the x axis, where q is the elementary charge. It corresponds to the acceleration induced by an electrostatic field of amplitude E . We take $m_{\text{Na}} = 22.990$ g mol $^{-1}$ and

$$m_{\text{Cl}} = 35.450 \text{ g mol}^{-1}.$$

For each run, we measure the average velocity of the anions v_{Cl} and cations v_{Na} after dropping the first nanosecond of the run and we compute the conductivity with

$$\sigma(E) = \frac{q\rho(v_{\text{Na}} - v_{\text{Cl}})}{E}. \quad (\text{A3})$$

with ρ the ionic density.

4. Estimation of the ion mobility

We use a very dilute regime to compute the mobility of the ions. We simulate a cubic box of aqueous electrolyte of side $L = 10$ nm. The 10 mM solution contains 6 pairs of (Na^+ , Cl^-) and 32761 water molecules. After equilibration following the procedure described in subsection A 1, we perform a simulation run of 40 ns and evaluate the diffusion coefficient of the ions from the mean square displacement using the command “gmx msd”. We obtain $D_{\text{Na}} = 1.2813(3351) \times 10^{-9}$ m 2 /s and $D_{\text{Cl}} = 2.0514(2811) \times 10^{-9}$ m 2 /s. We calculate mobilities using the Einstein relation $\kappa_i = D_i/k_B T$:

$$\kappa_{\text{Na}} = 3.0935(8090) \times 10^{11} \text{ m s}^{-1} \text{ N}^{-1}, \quad (\text{A4})$$

$$\kappa_{\text{Cl}} = 4.9527(6787) \times 10^{11} \text{ m s}^{-1} \text{ N}^{-1}. \quad (\text{A5})$$

5. Statistical treatment

For the parallel and perpendicular permittivity (Eqs. (A1,A2)) and for the conductivity (Eq. (A3)), we compute the error bars with the reblocking method [43].

Appendix B: Correlations from SDF T

Ionic correlations have been computed for arbitrary interactions in Ref. [14]. The operators $\tilde{R}(\mathbf{k})$ and $\tilde{A}(\mathbf{k})$ of Eqs. (15, 16) in Ref. [14] are given by

$$\tilde{R}(\mathbf{k}) = k^2 \begin{pmatrix} \bar{\rho}_+ \kappa_+ & 0 \\ 0 & \bar{\rho}_- \kappa_- \end{pmatrix} = k^2 \begin{pmatrix} r_+ & 0 \\ 0 & r_- \end{pmatrix}, \quad (\text{B1})$$

$$\tilde{A}(\mathbf{k}) = T \begin{pmatrix} \frac{1}{\bar{\rho}_+} \left(1 + i \frac{z_+ q \mathbf{E} \cdot \mathbf{k}}{T k^2} \right) + \frac{\tilde{V}_{++}(\mathbf{k})}{T} & \frac{\tilde{V}_{+-}(\mathbf{k})}{T} \\ \frac{\tilde{V}_{+-}(\mathbf{k})}{T} & \frac{1}{\bar{\rho}_-} \left(1 + i \frac{z_- q \mathbf{E} \cdot \mathbf{k}}{T k^2} \right) + \frac{\tilde{V}_{--}(\mathbf{k})}{T} \end{pmatrix} = T \begin{pmatrix} a & b \\ b & c \end{pmatrix}. \quad (\text{B2})$$

We still use electrostatic interactions:

$$\tilde{V}_{\alpha\beta}(\mathbf{k}) = q^2 z_{\alpha} z_{\beta} \tilde{G}_0(\mathbf{k}), \quad (\text{B3})$$

where here

$$\tilde{G}_0(\mathbf{k}) = \frac{1}{\epsilon(\alpha_{\parallel} k_{\parallel}^2 + \alpha_{\perp} k_{\perp}^2)} = \frac{\tilde{g}(\mathbf{k})}{\epsilon}. \quad (\text{B4})$$

$$\tilde{C} = \frac{2}{(a+a^*)(c+c^*)|r_+a+r_-c^*|^2 - b^2[r_+(a+a^*)+r_-(c+c^*)]^2} \times \begin{pmatrix} (c+c^*)|r_+a+r_-c^*|^2 & -b(r_+a^*+r_-c)[r_+(a+a^*)+r_-(c+c^*)] \\ -b(r_+a+r_-c^*)[r_+(a+a^*)+r_-(c+c^*)] & (a+a^*)|r_+a+r_-c^*|^2 \end{pmatrix}. \quad (\text{B5})$$

We define

$$\kappa = \kappa_+ + \kappa_-, \quad (\text{B6})$$

$$\kappa' = \kappa_+z_+ - \kappa_-z_-, \quad (\text{B7})$$

$$m_\alpha^2 = \frac{q^2 z_\alpha^2 \bar{\rho}_\alpha}{\epsilon T}, \quad (\text{B8})$$

$$m^2 = m_+^2 + m_-^2, \quad (\text{B9})$$

$$m'^2 = \frac{\kappa_+ m_+^2 + \kappa_- m_-^2}{\kappa_+ + \kappa_-} = \frac{\sigma_0}{\epsilon T(\kappa_+ + \kappa_-)}, \quad (\text{B10})$$

$$F = \frac{qE}{mT} = \frac{E}{E_c}. \quad (\text{B11})$$

We find

$$\tilde{C} = \left[\kappa^2(1+m^2\tilde{g})(1+m'^2\tilde{g})^2 + \kappa'^2 m^2(1+m_+^2\tilde{g})(1+m_-^2\tilde{g}) \left(\frac{Fk_\parallel}{k^2} \right)^2 \right]^{-1} \times \begin{pmatrix} \bar{\rho}_+(1+m_-^2\tilde{g}) \left[\kappa^2(1+m'^2\tilde{g})^2 + \kappa'^2 m^2 \left(\frac{Fk_\parallel}{k^2} \right)^2 \right] & \sqrt{\bar{\rho}_+\bar{\rho}_-} \kappa m_+ m_- \tilde{g} (1+m'^2\tilde{g}) \left[\kappa(1+m'^2\tilde{g}) - i\kappa' m \frac{Fk_\parallel}{k^2} \right] \\ \sqrt{\bar{\rho}_+\bar{\rho}_-} \kappa m_+ m_- \tilde{g} (1+m'^2\tilde{g}) \left[\kappa(1+m'^2\tilde{g}) + i\kappa' m \frac{Fk_\parallel}{k^2} \right] & \bar{\rho}_-(1+m_+^2\tilde{g}) \left[\kappa^2(1+m'^2\tilde{g})^2 + \kappa'^2 m^2 \left(\frac{Fk_\parallel}{k^2} \right)^2 \right] \end{pmatrix} \quad (\text{B12})$$

Appendix C: Electrostatic correction to the conductivity

1. General case

Using Eq. (25) in [14], we find the electrostatic correction to the conductivity:

$$\frac{\Delta\sigma}{\sigma_0} = \frac{q^3}{\sigma_0 \epsilon E} \sum_{\alpha,\beta} \kappa_\alpha z_\alpha^2 z_\beta \int ik_\parallel \tilde{g} \tilde{C}_{\alpha\beta}(\mathbf{k}) \frac{d\mathbf{k}}{(2\pi)^d} \quad (\text{C1})$$

$$= -\frac{q^2 \kappa'^2 m_+^2 m_-^2}{\epsilon T m'^2} \int \frac{k_\parallel^2 \tilde{g}^2 (1+m'^2\tilde{g})}{k^2 \left[\kappa^2(1+m^2\tilde{g})(1+m'^2\tilde{g})^2 + \kappa'^2 m^2(1+m_+^2\tilde{g})(1+m_-^2\tilde{g}) \left(\frac{Fk_\parallel}{k^2} \right)^2 \right]} \frac{d\mathbf{k}}{(2\pi)^d}. \quad (\text{C2})$$

To integrate the correction numerically, we specify the calculation to $d=3$ and we change the integration variable from \mathbf{k} to $u \in [0, \infty)$ and $z \in [-1, 1]$ with $\mathbf{k} = m\mathbf{u}$ and $z = u_\parallel/u$, $d\mathbf{k} = 2\pi m^3 u^2 du dz$. The Green function reads $\tilde{g} = (m^2 u^2 \alpha_z)^{-1}$ (Eq. (B4)) and the correction is given by

$$\frac{\Delta\sigma}{\sigma_0} = -\frac{q^2 m_+^2 m_-^2 m^3}{(2\pi)^2 \epsilon T m'^2} \int_0^\infty du \int_{-1}^1 dz \frac{z^2 u^2 \tilde{g}^2 (1+m'^2\tilde{g})}{\frac{\kappa^2}{\kappa'^2} (1+m^2\tilde{g})(1+m'^2\tilde{g})^2 + (1+m_+^2\tilde{g})(1+m_-^2\tilde{g}) \frac{F^2 z^2}{u^2}} \quad (\text{C3})$$

$$= -\frac{q^2 m \mu_+^2 \mu_-^2}{(2\pi)^2 \epsilon T m'^2} \int_0^\infty du \int_{-1}^1 dz \frac{z^2 \left(1 + \frac{\mu'^2}{u^2 \alpha_z} \right)}{\alpha_z^2 u^2 \left[\frac{\kappa^2}{\kappa'^2} \left(1 + \frac{1}{u^2 \alpha_z} \right) \left(1 + \frac{\mu'^2}{u^2 \alpha_z} \right)^2 + \left(1 + \frac{\mu_+^2}{u^2 \alpha_z} \right) \left(1 + \frac{\mu_-^2}{u^2 \alpha_z} \right) \frac{F^2 z^2}{u^2} \right]} \quad (\text{C4})$$

$$= -\frac{q^2 m \mu_+^2 \mu_-^2}{2\pi^2 \epsilon T m'^2} \int_0^\infty du \int_0^1 dz \frac{z^2 u^2 (\alpha_z u^2 + \mu'^2)}{\frac{\kappa^2}{\kappa'^2} (\alpha_z u^2 + 1) (\alpha_z u^2 + \mu'^2)^2 + F^2 z^2 \alpha_z (\alpha_z u^2 + \mu_+^2) (\alpha_z u^2 + \mu_-^2)}. \quad (\text{C5})$$

We have introduced $\mu' = m'/m$, $\mu_\pm = m_\pm/m$, and used the fact that the integral is even in z .

2. Monovalent salt

For a monovalent salt, $z_+ = -z_- = 1$ and $\rho_+ = \rho_-$, so that $m_i^2 = m'^2 = m^2/2$, $\kappa' = \kappa$, $\mu_i = \mu' = 1/\sqrt{2}$. The expression above simplifies to

$$\frac{\Delta\sigma_{\text{el}}}{\sigma_0} = -\frac{\beta q^2 m}{2\pi^2 \epsilon_0 \epsilon_r} \int_0^\infty du \int_0^1 dz \frac{z^2 u^2}{(2u^2 \alpha_z + 1)(u^2 \alpha_z + 1 + F^2 z^2 \alpha_z)} \quad (\text{C6})$$

The integral over u can be performed analytically, leading to

$$\frac{\Delta\sigma_{\text{el}}}{\sigma_0} = -\frac{\beta q^2 m}{4\sqrt{2}\pi\epsilon_0\epsilon_r} \int_0^1 \frac{z^2 dz}{\alpha_z^{3/2} [1 + \sqrt{2}(1 + F^2 z^2 \alpha_z)]}. \quad (\text{C7})$$

3. Small field expansion

We write the electrostatic correction as

$$\frac{\Delta\sigma_{\text{el}}}{\sigma_0} = -\frac{\beta q^2 m \mu_+^2 \mu_-^2}{2\pi^2 \epsilon_0 \epsilon_r \mu'^2} s_e, \quad (\text{C8})$$

with

$$s_e = \int_0^\infty du \int_0^1 dz \frac{z^2 u^2 (\alpha_z u^2 + \mu'^2)}{\frac{\kappa^2}{\kappa'^2} (\alpha_z u^2 + 1) (\alpha_z u^2 + \mu'^2)^2 + F^2 z^2 \alpha_z (\alpha_z u^2 + \mu_+^2) (\alpha_z u^2 + \mu_-^2)}. \quad (\text{C9})$$

After a few lines of calculation, we get at order E^2

$$s_e = \frac{\kappa'^2}{3\kappa^2} \int_0^\infty du \frac{u^2}{(1+u^2)(u^2+\mu'^2)} - \frac{\kappa'^4}{5\kappa^4} F^2 \int_0^\infty du \frac{u^2(u^2+\mu_+^2)(u^2+\mu_-^2)}{(u^2+1)^2(u^2+\mu'^2)^3} + \frac{11}{225} \frac{\kappa'^2}{\kappa^2} \frac{\epsilon_r - 1}{\epsilon_r} x^2 \int_0^\infty du \frac{u^4(2u^2+1+\mu'^2)}{(u^2+1)^2(u^2+\mu'^2)^2}, \quad (\text{C10})$$

where $F = E/E_c$ and $x = E/E_w$.

Appendix D: Hydrodynamic correction to the conductivity

1. General case

The hydrodynamic correction to the conductivity is [37] (Eq. (17)):

$$\frac{\Delta\sigma_{\text{hyd}}}{\sigma_0} = q^2 \int \tilde{\mathcal{O}}_{11}(\mathbf{k}) \sum_{\alpha\beta} z_\alpha z_\beta \left[\tilde{C}_{\alpha\beta}(\mathbf{k}) - \bar{\rho}_\alpha \delta_{\alpha\beta} \right] \frac{d\mathbf{k}}{(2\pi)^d}. \quad (\text{D1})$$

Using the correlation (B12), we find

$$\begin{aligned} \frac{\Delta\sigma_{\text{hyd}}}{\sigma_0} &= -\frac{q^2}{\eta\sigma_0} \int \frac{d\mathbf{k}}{(2\pi)^d} \frac{k_\perp^2}{k^4} \tilde{g} \\ &\times \frac{\kappa^2 (1 + m'^2 \tilde{g})^2 (z_+ \sqrt{\bar{\rho}_+} m_+ + z_- \sqrt{\bar{\rho}_-} m_-)^2 + \kappa'^2 m^2 [z_+^2 \bar{\rho}_+ m_+^2 (1 + m_-^2 \tilde{g}) + z_-^2 \bar{\rho}_- m_-^2 (1 + m_+^2 \tilde{g})] \left(\frac{F k_\parallel}{k^2}\right)^2}{\kappa^2 (1 + m^2 \tilde{g})(1 + m'^2 \tilde{g})^2 + \kappa'^2 m^2 (1 + m_+^2 \tilde{g})(1 + m_-^2 \tilde{g}) \left(\frac{F k_\parallel}{k^2}\right)^2}. \end{aligned} \quad (\text{D2})$$

To perform the numerical integration, we follow the same steps as for the electrostatic correction:

$$\begin{aligned} \frac{\Delta\sigma_{\text{hyd}}}{\sigma_0} &= -\frac{q^2 m}{(2\pi)^2 \eta \sigma_0} \int_0^\infty du \int_{-1}^1 dz (1-z^2) \tilde{g} \\ &\times \frac{\frac{\kappa^2}{\kappa'^2} (1+m'^2 \tilde{g})^2 (\sum_\alpha z_\alpha \sqrt{\rho_\alpha} m_\alpha)^2 + [z_+^2 \bar{\rho}_+ m_+^2 (1+m_-^2 \tilde{g}) + z_-^2 \bar{\rho}_- m_-^2 (1+m_+^2 \tilde{g})] \frac{F^2 z^2}{u^2}}{\frac{\kappa^2}{\kappa'^2} (1+m'^2 \tilde{g})(1+m'^2 \tilde{g})^2 + (1+m_+^2 \tilde{g})(1+m_-^2 \tilde{g}) \frac{F^2 z^2}{u^2}} \end{aligned} \quad (\text{D3})$$

$$\begin{aligned} &= -\frac{q^2 m}{(2\pi)^2 \eta \sigma_0} \int_0^\infty du \int_{-1}^1 dz \frac{1-z^2}{u^2 \alpha_z} \\ &\times \frac{\frac{\kappa^2}{\kappa'^2} \left(1 + \frac{\mu'^2}{u^2 \alpha_z}\right)^2 (\sum_\alpha z_\alpha \sqrt{\rho_\alpha} \mu_\alpha)^2 + \left[z_+^2 \bar{\rho}_+ \mu_+^2 \left(1 + \frac{\mu_-^2}{u^2 \alpha_z}\right) + z_-^2 \bar{\rho}_- \mu_-^2 \left(1 + \frac{\mu_+^2}{u^2 \alpha_z}\right)\right] \frac{F^2 z^2}{u^2}}{\frac{\kappa^2}{\kappa'^2} \left(1 + \frac{1}{u^2 \alpha_z}\right) \left(1 + \frac{\mu'^2}{u^2 \alpha_z}\right)^2 + \left(1 + \frac{\mu_+^2}{u^2 \alpha_z}\right) \left(1 + \frac{\mu_-^2}{u^2 \alpha_z}\right) \frac{F^2 z^2}{u^2}} \end{aligned} \quad (\text{D4})$$

$$\begin{aligned} &= -\frac{q^2 m}{2\pi^2 \eta \sigma_0} \int_0^\infty du \int_0^1 dz (1-z^2) \\ &\times \frac{\frac{\kappa^2}{\kappa'^2} (u^2 \alpha_z + \mu'^2)^2 (\sum_\alpha z_\alpha \sqrt{\rho_\alpha} \mu_\alpha)^2 + F^2 z^2 \alpha_z [z_+^2 \bar{\rho}_+ \mu_+^2 (u^2 \alpha_z + \mu_-^2) + z_-^2 \bar{\rho}_- \mu_-^2 (u^2 \alpha_z + \mu_+^2)]}{\frac{\kappa^2}{\kappa'^2} (u^2 \alpha_z + 1)(u^2 \alpha_z + \mu'^2)^2 + F^2 z^2 \alpha_z (u^2 \alpha_z + \mu_+^2)(u^2 \alpha_z + \mu_-^2)}. \end{aligned} \quad (\text{D5})$$

2. Monovalent salt

For a monovalent salt the expression above simplifies into

$$\frac{\Delta\sigma_{\text{hyd}}}{\sigma_0} = -\frac{m}{\pi^2 \eta \kappa} \int_0^\infty du \int_0^1 dz \frac{(1-z^2)(2u^2 \alpha_z + 1 + F^2 z^2 \alpha_z)}{(2u^2 \alpha_z + 1)(u^2 \alpha_z + 1 + F^2 z^2 \alpha_z)}. \quad (\text{D6})$$

The integral over u can be performed analytically, leading to

$$\frac{\Delta\sigma_{\text{hyd}}}{\sigma_0} = -\frac{m}{2\sqrt{2}\pi\eta\kappa} \int_0^1 dz \frac{1-z^2}{\sqrt{\alpha_z}} \left[1 + \frac{1}{1 + \sqrt{2(1 + F^2 z^2 \alpha_z)}} \right]. \quad (\text{D7})$$

3. Small field expansion

For the hydrodynamic correction, we denote

$$\frac{\Delta\sigma_{\text{hyd}}}{\sigma_0} = -\frac{q^2 m}{2\pi^2 \eta \sigma_0} s_h, \quad (\text{D8})$$

where

$$\begin{aligned} s_h &= \int_0^\infty du \int_0^1 dz (1-z^2) \\ &\times \frac{\frac{\kappa^2}{\kappa'^2} (u^2 \alpha_z + \mu'^2)^2 (\sum_i z_i \sqrt{\rho_i} \mu_i)^2 + F^2 z^2 \alpha_z [z_+^2 \bar{\rho}_+ \mu_+^2 (u^2 \alpha_z + \mu_-^2) + z_-^2 \bar{\rho}_- \mu_-^2 (u^2 \alpha_z + \mu_+^2)]}{\frac{\kappa^2}{\kappa'^2} (u^2 \alpha_z + 1)(u^2 \alpha_z + \mu'^2)^2 + F^2 z^2 \alpha_z (u^2 \alpha_z + \mu_+^2)(u^2 \alpha_z + \mu_-^2)}. \end{aligned} \quad (\text{D9})$$

Using the same approach, we find at order E^2

$$\begin{aligned} s_h &= \frac{\pi}{3} \left(\sum_i \sqrt{z_i^2 \mu_i^2 \rho_i} \right)^2 + \frac{7\pi}{450} \frac{\epsilon_r - 1}{\epsilon_r} \left(\sum_i \sqrt{z_i^2 \mu_i^2 \rho_i} \right)^2 x^2 \\ &+ \frac{2}{15} \frac{\kappa'^2}{\kappa^2} F^2 \left[\int_0^\infty du \frac{z_+^2 \bar{\rho}_+ \mu_+^2 (u^2 + \mu_-^2) + z_-^2 \bar{\rho}_- \mu_-^2 (u^2 + \mu_+^2)}{(u^2 + 1)(u^2 + \mu'^2)^2} - \left(\sum_i \sqrt{z_i^2 \mu_i^2 \rho_i} \right)^2 \int_0^\infty du \frac{(u^2 + \mu_+^2)(u^2 + \mu_-^2)}{(u^2 + 1)^2 (u^2 + \mu'^2)^2} \right], \end{aligned} \quad (\text{D10})$$

where $F = E/E_c$ and $x = E/E_w$.

-
- [1] H. C. Eckstrom and C. Schmelzer, *Chemical Reviews* **24**, 367 (1939).
- [2] J. Feng, K. Liu, M. Graf, D. Dumcenco, A. Kis, M. Di Ventra, and A. Radenovic, *Nature Materials* **15**, 850 (2016).
- [3] J. Cai, E. Griffin, V. H. Guarochico-Moreira, D. Barry, B. Xin, M. Yagmurcukardes, S. Zhang, A. K. Geim, F. M. Peeters, and M. Lozada-Hidalgo, *Nature Communications* **13**, 5776 (2022).
- [4] A. Montenegro, C. Dutta, M. Mammetkuliev, H. Shi, B. Hou, D. Bhattacharyya, B. Zhao, S. B. Cronin, and A. V. Benderskii, *Nature* **594**, 62 (2021).
- [5] P. Robin, T. Emmerich, A. Ismail, A. Niguès, Y. You, G.-H. Nam, A. Keerthi, A. Siria, A. K. Geim, B. Radha, and L. Bocquet, *Science* **379**, 161 (2023).
- [6] P. Robin, N. Kavokine, and L. Bocquet, *Science* **373**, 687 (2021).
- [7] W. S. Wilson, *The theory of the Wien effect for a binary electrolyte*, Ph.D. thesis, Yale University (1936).
- [8] P. Debye and E. Hückel, *Physikalische Zeitschrift* **24**, 305 (1923).
- [9] L. Onsager, *Transactions of the Faraday Society* **23**, 341 (1927).
- [10] L. Onsager and S. K. Kim, *The Journal of Physical Chemistry* **61**, 198 (1957).
- [11] D. Lesnicki, C. Y. Gao, B. Rotenberg, and D. T. Limmer, *Phys. Rev. Lett.* **124**, 206001 (2020).
- [12] D. Lesnicki, C. Y. Gao, D. T. Limmer, and B. Rotenberg, *The Journal of Chemical Physics* **155**, 014507 (2021).
- [13] D. S. Dean, *Journal of Physics A: Mathematical and General* **29**, L613 (1996).
- [14] V. Démery and D. S. Dean, *Journal of Statistical Mechanics: Theory and Experiment* **2016**, 023106 (2016).
- [15] J.-P. Péraud, A. J. Nonaka, J. B. Bell, A. Donev, and A. L. Garcia, *Proceedings of the National Academy of Sciences* **114**, 10829 (2017).
- [16] A. Donev, A. L. Garcia, J.-P. Péraud, A. J. Nonaka, and J. B. Bell, *Current Opinion in Electrochemistry* **13**, 1 (2019).
- [17] Y. Avni, R. M. Adar, D. Andelman, and H. Orland, *Phys. Rev. Lett.* **128**, 098002 (2022).
- [18] Y. Avni, D. Andelman, and H. Orland, *The Journal of Chemical Physics* **157**, 154502 (2022).
- [19] O. Bernard, M. Jardat, B. Rotenberg, and P. Illien, *The Journal of Chemical Physics* **159**, 164105 (2023).
- [20] J.-F. Dufrière, O. Bernard, S. Durand-Vidal, and P. Turq, *The Journal of Physical Chemistry B* **109**, 9873 (2005), pMID: 16852194.
- [21] F. Booth, *The Journal of Chemical Physics* **19**, 391 (1951).
- [22] A. Piekara and S. Kielich, *The Journal of Chemical Physics* **29**, 1297 (1958).
- [23] I.-C. Yeh and M. L. Berkowitz, *The Journal of Chemical Physics* **110**, 7935 (1999).
- [24] H. A. Kotodziej, G. P. Jones, and M. Davies, *J. Chem. Soc., Faraday Trans. 2* **71**, 269 (1975).
- [25] E. N. D. C. Andrade and C. Dodd, *Proceedings of the Royal Society of London. Series A. Mathematical and Physical Sciences* **187**, 296 (1946).
- [26] J. Lyklema and J. Overbeek, *Journal of Colloid Science* **16**, 501 (1961).
- [27] D. Zong, H. Hu, Y. Duan, and Y. Sun, *J. Phys. Chem. B* **120**, 4818 (2016).
- [28] D. Jin, Y. Hwang, L. Chai, N. Kampf, and J. Klein, *Proceedings of the National Academy of Sciences* **119**, e2113690119 (2022).
- [29] A. Abrashkin, D. Andelman, and H. Orland, *Phys. Rev. Lett.* **99**, 077801 (2007).
- [30] H. J. C. Berendsen, J. R. Grigera, and T. P. Straatsma, *J. Phys. Chem.* **91**, 6269 (1987).
- [31] P. E. Smith and W. F. van Gunsteren, *Chemical Physics Letters* **215**, 315 (1993).
- [32] P. Loche, P. Steinbrunner, S. Friedowitz, R. R. Netz, and D. J. Bonhuis, *J. Phys. Chem. B* **125**, 8581 (2021).
- [33] B. Hess, C. Kutzner, D. van der Spoel, and E. Lindahl, *J. Chem. Theory Comput.* **4**, 435 (2008).
- [34] R. L. Fulton, *The Journal of Chemical Physics* **130**, 204503 (2009).
- [35] H. Berthoumieux, G. Monet, and R. Blossey, *J. Chem Phys.* **155**, 024112 (2021).
- [36] L. D. Landau, J. S. Bell, M. Kearsley, L. Pitaevskii, E. Lifshitz, and J. Sykes, *Electrodynamics of continuous media*, Vol. 8 (elsevier, 2013).
- [37] H. Bonneau, V. Démery, and E. Raphaël, *Journal of Statistical Mechanics: Theory and Experiment* **2023**, 073205 (2023).
- [38] H. Berthoumieux, *The Journal of Chemical Physics* **148**, 104504 (2018).
- [39] H. Jalali, E. Lofte, R. Boya, and M. Neek-Amal, *J. Phys. Chem. B* **125**, 1604 (2021).
- [40] P. Loche, C. Ayaz, A. Schlaich, Y. Uematsu, and R. R. Netz, *J. Phys. Chem. B* **123**, 10850 (2019).
- [41] L. Fumagalli, A. Esfandiar, R. Fabregas, S. Hu, P. Ares, A. Janardanan, Q. Yang, B. Rhada, T. Tanigushi, K. Watanabe, G. Gomila, K. S. Novoselov, and A. K. Geim, *Science* **360**, 1339 (2018).
- [42] M. Neumann, *Mol. Phys.* **50**, 841 (1983).
- [43] H. Flyvbjerg and H. G. Petersen, *The Journal of Chemical Physics* **91**, 461 (1989).